PHYSICAL REVIEW B **88**, 205112 (2013)

Connecting bulk symmetry and orbital polarization in strained $RNiO_3$ ultrathin films

I. C. Tung,[1,2,*] P. V. Balachandran,[3] Jian Liu,[4,5,†] B. A. Gray,[4] E. A. Karapetrova,[1] J. H. Lee,[1] J. Chakhalian,[4]
M. J. Bedzyk,[2] J. M. Rondinelli,[3] and J. W. Freeland[1,‡]
[1]*Advanced Photon Source, Argonne National Laboratory, Argonne, Illinois 60439, USA*
[2]*Department of Materials Science and Engineering, Northwestern University, Evanston, Illinois 60208, USA*
[3]*Department of Materials Science & Engineering, Drexel University, Philadelphia, Pennsylvania 19104, USA*
[4]*Department of Physics, University of Arkansas, Fayetteville, Arkansas 70701, USA*
[5]*Advanced Light Source, Lawrence Berkeley National Laboratory, Berkeley, California 94720, USA*
(Received 22 February 2013; revised manuscript received 10 October 2013; published 12 November 2013)

We examine the structural and electronic properties of $LaNiO_3$ and $NdNiO_3$ *epitaxial thin films* grown on cubic (001) $SrTiO_3$ from the viewpoint of *bulk* crystal symmetry and misfit strain. X-ray scattering and polarization-dependent x-ray absorption spectroscopy measurements are performed to determine the crystal symmetry and extract the local Ni $3d$ orbital response, respectively, to understand the strain-induced distortions of the bulk structure. A strain-induced orbital polarization is found in $NdNiO_3$ films, but is absent in $LaNiO_3$ films. The difference in electronic structure is attributed to the bulk thermodynamic phases through group theoretical methods, which reveals that thin film perovskites retain a "memory" of their preferred electronic and structural configurations.

DOI: 10.1103/PhysRevB.88.205112 PACS number(s): 73.20.−r, 61.05.cj

I. INTRODUCTION

Owing to the remarkable progress in achieving high-quality coherent perovskite oxide thin films and superlattices, heteroepitaxial synthesis has evolved into a reliable strategy to engineer orbital-lattice interactions in correlated oxide materials.[1,2] In ultrathin film perovskite oxides, strain fields at the thin film-substrate interface directly tune the local electronic states of the correlated transition metal (TM) d orbitals, from which novel functionalities and phases prohibited in bulk phases are stabilized.[3–5] Rotationally distorted ABO_3 oxides, in particular, are susceptible to strain-induced changes in bond lengths and bond angles, which modify the crystal field symmetry and lead to differential orbital occupation (polarization). However, despite the recent progress, there is very limited experimental understanding of factors conducive to large orbital polarizations.[6–10] What governs the orbital-lattice response of the BO_6 units to the substrate-induced heteroepitaxial constraints? Isolating the principal interactions remains challenging: The orbital occupation can be significantly influenced by elastic strain (substrate-film lattice mismatch), octahedral rotation dissimilarities (crystallographic symmetry mismatch), and electrostatic (polarity) mismatch.[11]

In this paper, we experimentally demonstrate that the *bulk* crystal symmetry directs the atomic and orbital responses adopted by a coherently strained ultrathin film of perovskites. Using $RNiO_3$ perovskite nickelate thin films (R = rare-earth, i.e., La and Nd) on cubic $SrTiO_3$ (STO) substrates, in particular, we isolate the role of the parent crystal's symmetry on the orbital-lattice evolution. Detailed x-ray crystal truncation rod (CTR) measurements and x-ray linear dichroism (XLD) show that tensile strain generates a small orbital splitting consistent with out-of-plane lattice contraction for nominally *orthorhombic* $NdNiO_3$ (NNO) films, while no experimentally observable orbital splitting is found in *monoclinic* $LaNiO_3$ (LNO) films, which also exhibit a comparable tetragonal lattice contraction. We trace the key feature to the symmetry unique NiO_6 octahedral distortions present in the bulk NNO and LNO phases, which produce distinct rotational patterns in thin films identified from a systematic survey of the half-order Bragg reflections. A quantitative group theoretical analysis of the epitaxial stabilized crystal structures computed from density functional theory (DFT) reveals that the preferred orbital configurations adopted by the thin films is the one that stays closest to the bulk, suggesting the strain-stabilized phases maintain a "memory" of their bulk state. Knowledge of the structural distortions present in the bulk thermodynamic phases emerges as a simple descriptor to guide materials selection for epitaxial thin films with designed large orbital polarizations.

We chose to study the correlated $RNiO_3$ system, which exhibits a bandwidth-controlled metal-insulator transition (MIT)[12] driven by changes in the Ni-O-Ni structure with pressure,[13] different size R cations,[14] and epitaxial strain.[15,16] Rhombohedral $LaNiO_3$ (LNO) and orthorhombic $NdNiO_3$ (NNO) are selected because in bulk at room temperature (RT), both compounds are metallic (nominal Ni^{3+} valence) and are only distinguished by their different crystal structures: LNO exhibits out-of-phase NiO_6 octahedral rotations about the three-fold axis along the pseudocubic [111] direction ($a^-a^-a^-$ in Glazer notation, space group $R\bar{3}c$), and NNO is orthorhombic with one in-phase and two out-of-phase octahedral rotations ($a^-a^-c^+$, space group $Pbnm$), as illustrated in Fig. 1.[17] Ultrathin films of 10–15 unit cell (uc) thickness with a 2 uc $LaAlO_3$ (LAO) buffer layer[18] were synthesized on TiO_2-terminated (001)-oriented STO substrates by pulsed laser deposition (PLD) with *in-situ* monitoring by reflection high energy electron diffraction (RHEED). The fixed sign of the lattice mismatch due to the STO substrate—both LNO and NNO are subjected to a tensile strain of 1.8% and 2.6%, respectively—allows us to isolate the contribution of the bulk symmetry difference (rhombohedral versus orthorhombic *vis á vis* the three or two out-of-phase rotations) on the orbitally polarized ground states.

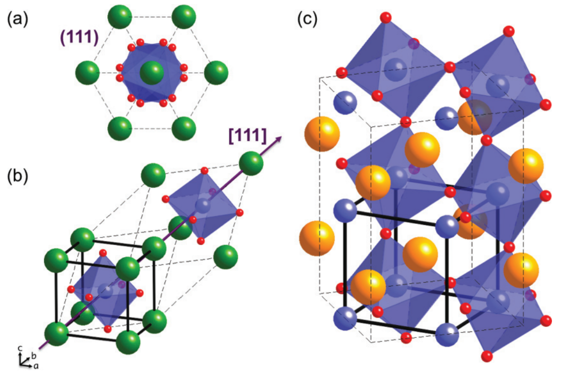

FIG. 1. (Color online) Schematic of the bulk $LaNiO_3$ [(a),(b)] and $NdNiO_3$ [(c)] structures showing both rhombohedral ($R\bar{3}c$) unit cell (dashed line) and orthorhombic ($Pbmn$) unit cell (dashed line) and the relationship to the pseudocubic unit cell (solid line). Part of the oxygen atoms and octahedra are not shown in (c) for clarity. La atoms shown in green; Nd atoms shown in orange; Ni atoms shown in blue at center of oxygen (red) octahedra.

II. EXPERIMENTS

Coherent epitaxy, confirmed by reciprocal space mapping, and proper composition of the thin films is maintained during the layer-by-layer growth with the interrupted deposition approach[19] on single crystal STO substrates with TiO_2-terminated (001) surfaces prepared by a chemical wet-etch procedure.[20] The growth temperature was set in the range of 730–780 °C for LNO and 670–730 °C for NNO, while the oxygen partial pressure is maintained at 75–120 mTorr. After deposition, the samples are post-annealed *in-situ* for 30 minutes and cooled down to room temperature in one atmosphere of ultrapure oxygen to maintain the proper oxygen content.[15] The film structures were studied by x-ray scattering experiments in air at room temperature with standard four-circle diffractometers performed at beamlines 5-BM-D and 33-BM-C of the Advanced Photon Source (APS) at Argonne National Laboratory. The electronic and orbital properties of the samples were obtained with polarized soft x-ray absorption (beamline 4-ID-C of the APS) acquired in the bulk sensitive fluorescence yield (FY) mode with a NiO (Ni^{2+}) standard measured simultaneously in the diagnostic section of beamline 4-ID-C for spectral alignment.[21]

III. RESULTS AND DISCUSSIONS

A. Structure analysis

Figure 2 shows the specular x-ray reflectivity data (dots) with error bar along the (00L) crystal truncation rod (CTR) for the NNO/LAO/STO (001) and LNO/LAO/STO (001) heterolayer structures. A ridge scan was used to acquire the specular scattering profile in the vicinity of the STO (002) peak as a function of out-of-plane scattering vector Q_z. The background was subtracted from the reflectivity data by measuring rocking curves at several points along the scan,[22] and a simulated curve (black line) was generated using a layered structural model. The $H = K$ reciprocal space maps (RSM) around the off-specular (113) Bragg peaks for the film and the substrate confirms both nickelate films are tetragonally strained and coherently lattice matched in-plane to the STO substrate [inset, Figs. 2(a) and 2(b)]. In addition, we found no evidence of lateral strain modulations, which has been observed in other oxide films and was related to strain accommodation.[23,24]

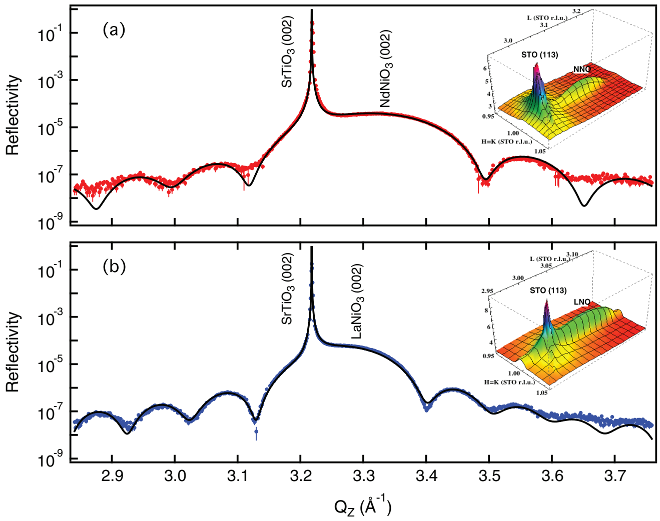

FIG. 2. (Color online) X-ray reflectivity data (dots) and fit (solid line) for scattering along the (00L) specular CTR through the $Q_z = 3.217$ Å^{-1} (002) Bragg peaks of the $SrTiO_3$ substrate and (a) $LaNiO_3$ and (b) $NdNiO_3$ film. Reciprocal space map around the (113) Bragg reflection showing the films are coherent with the STO substrate (inset).

Least-squares fitting was performed where the film structure parameters were allowed to vary while fitting various models to the data, but the bulk STO structure was fixed. The data points near the sharp STO (002) Bragg peak were omitted from fitting because the analysis only considers scattering in the kinematical approximation, and the data in this region do not contain information about the film structure itself. From the model-based analysis of the specular x-ray reflectivity, we experimentally determined that the unit cell thickness is $N = 12$ and 15 for NNO and LNO, and the out-of-plane lattice constants of NNO and LNO films are 3.760 ± 0.005 Å and 3.815 ± 0.005 Å,[16,25] respectively. The ranges of the upper and lower limit of the uncertainties of out-of-plane lattice parameters are determined from the $\Delta\chi^2 \sim 3$ contours[26] in the parameter space (90% confidence limits).[27] The results for NNO are consistent with an out-of-plane contraction, which is expected for a volume conserving scenario. Surprisingly, despite the fact that the LNO film was coherently strained by 1.8% tensile strain, the out-of-plane lattice constant is only 0.6% smaller than the bulk value. This anomalous lack of out-of-plane contraction is suggestive of a new structural phase with larger unit cell volume, which was reported previously.[7,28] Moreover it requires that the biaxial tensile strain is accommodated by both octahedral distortion and rotations perpendicular to the substrate or about an axis parallel to the substrate plane simultaneously or alternatively.[2]

To address why such a distinct lattice response exists between LNO and NNO, a systematic survey of the half-order Bragg peaks for both films was conducted to determine

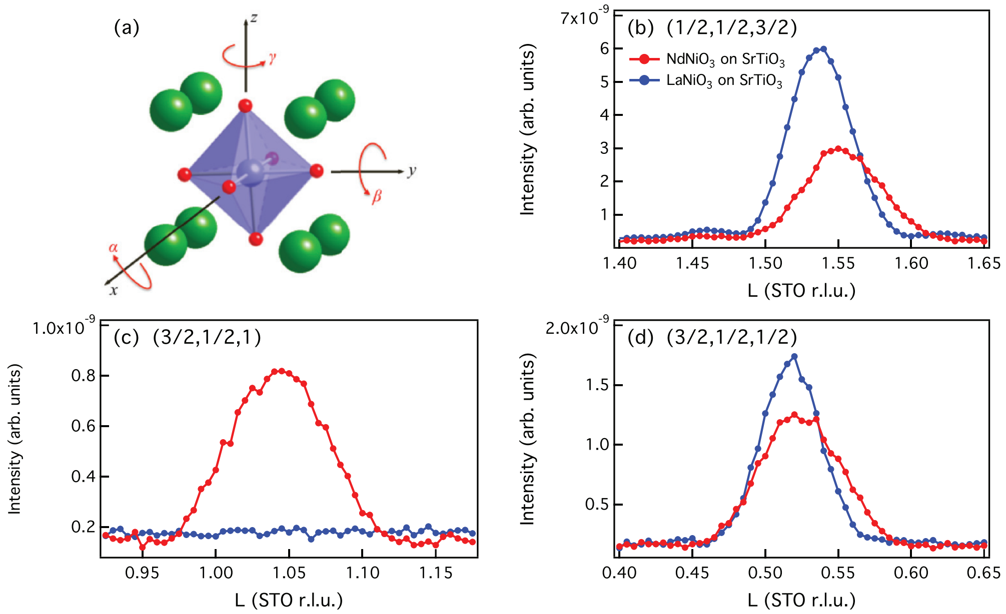

FIG. 3. (Color online) Half-order Bragg reflections through L at various H and K points. (a) A schematic illustration of the octahedral rotation axes. (b) $H = K = 1/2$; (c),(d) $H = 3/2$ and $K = 1/2$.

the octahedral rotations, distortions, and underlying crystal symmetry. Since the octahedral rotations effectively double the pseudocubic unit cell, extra Bragg reflections unique to each tilt system are expected at a distinctive set of half-order reciprocal-lattice points.[29] Consequently, we can identify the rotation pattern of the $\mathrm{RNiO_3}$ films by observing the presence and absence of specific half-order Bragg peaks.[30]

As anticipated, we find half-order peaks for both LNO and NNO films (Fig. 3), which confirms that heteroepitaxial growth on a cubic substrate does not suppress octahedral rotations even though they are likely modified in the first few unit cells of the film.[31,32] To identify the octahedral tilt pattern, we search for signature half-order peaks that arise from rotations along the three principle axes [Fig. 3(a)]. First, we examine in-plane rotations using the (1/2,1/2,3/2) reflection [Fig. 3(b)]. This peak implies that the in-plane unit cell is doubled from out-of-phase rotations for both LNO and NNO. To probe the out-of-plane rotations, we use peaks with integer L to determine the lack or presence of in-phase rotations along the film normal (z) direction. Fig. 3(c) shows the presence of a (3/2,1/2,1) Bragg peak for NNO but not for LNO, indicating the NNO film adopts the $a^-a^-c^+$ tilt pattern. To isolate the tilt pattern of LNO, we examine the (3/2,1/2,1/2) reflection [Fig. 3(d)], which contains information about rotations both in- and out-of-plane. The lack of integer L peak for LNO and reduction of the (3/2,1/2,1/2) peak height [Fig. 3(d)] with respect to the (1/2,1/2,3/2) peak [Fig. 3(b)] is consistent with an $a^-a^-c^-$ tilt pattern, where the out-of-plane tilts are reduced by the epitaxial strain.[28,33] From these tilt patterns, we conclude that LNO film has a lower monoclinic symmetry (space group $C2/c$) compared to the bulk LNO (rhombohedral, space group $R\bar{3}c$), consistent with earlier reports.[30] On the other hand, the NNO films remain in the same orthorhombic symmetry ($Pbnm$) as found in bulk at RT.

B. Electronic and orbital properties

To explore the link between structure and the local Ni orbital configuration, x-ray absorption spectra (XAS) of metallic NNO and LNO films on STO substrates were measured at the Ni L edge with linearly polarized x-ray to measure x-ray linear dichroism (XLD), i.e., the difference between out-of-plane and in-plane polarization absorption. With a grazing incidence angle of 15° and by setting the linear polarization from the undulator to be either parallel or perpendicular to the film plane, we use XLD to probe the local occupied $3d$ orbital symmetry and the delocalized states imposed from the coordinating oxygen ligands. From the polarization-averaged XAS (average of out-of-plane and in-plane polarization absorption), shown in Fig. 4, we quantitatively determine that the valence of Ni is identical to bulklike octahedrally coordinated $\mathrm{Ni^{3+}}$ testifying to the proper stoichiometry.[34]

First, consider the XAS of the NNO film [Fig. 5(a)]. The c-axis contraction shown by x-ray reflectivity ($c/a = 0.96$) clearly leads to a distortion of the octahedra as seen by an

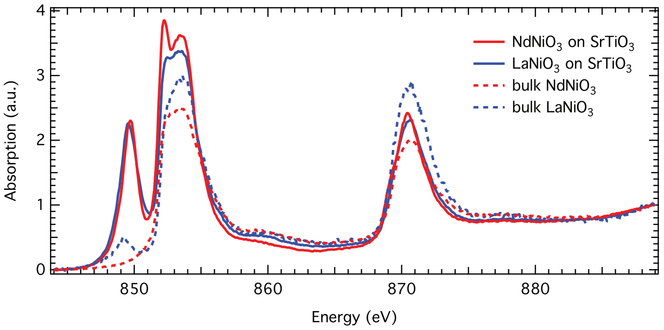

FIG. 4. (Color online) Polarization averaged XAS (average of out-of-plane and in-plane polarization absorption) measured in fluorescence yield (FY) mode at Ni L edge.

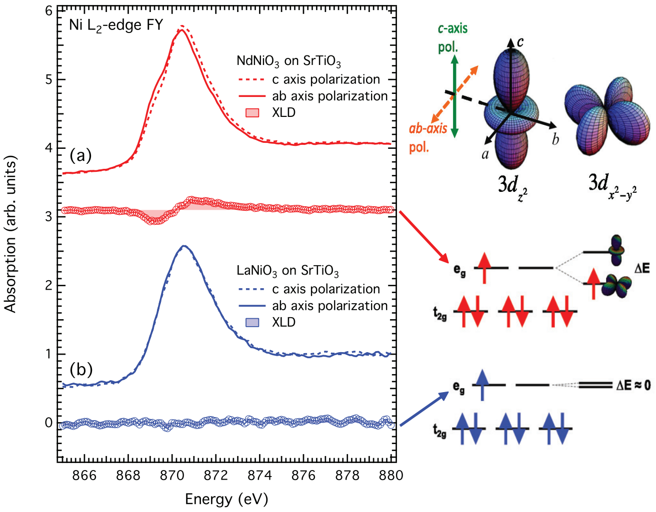

FIG. 5. (Color online) Polarization dependent x-ray absorption and x-ray linear dichroism (XLD) at the Ni L_2 edge for (a) NdNiO$_3$ and (b) LaNiO$_3$ on SrTiO$_3$. On the right, schematic orbital level diagram of NdNiO$_3$ on SrTiO$_3$ with the anticipated strain-induced orbital polarization effect on the e_g doublet and LaNiO$_3$ on SrTiO$_3$ without splitting of e_g orbitals. [Due to the overlap of M_4 edge of La (853 eV) with the Ni L_3 edge (852.7 eV), the spectra of films at the Ni L_3 edge is strongly distorted. Thus, the XLD was focused on the Ni L_2 edge (870 eV) where the line shape is free from distortions.]

increase of the c-axis d-orbital ($3d_{z^2}$) energy. The absorption for polarization perpendicular to the ab plane is shifted ~0.2 eV higher in energy than the in-plane polarization absorption [Fig. 5(a)]. The sign of the dichroism indicates a conduction band splitting ΔE between the e_g orbitals of Ni consistent with anisotropic Ni-O bonding, and it is in agreement with the strain-induced orbital polarization concept.[6,35] On the other hand, we would anticipate that the same orbital-lattice coupling should lead to an identical orbital polarization for LNO as in the case of NNO. However, our polarized XAS of the LNO film as shown in Fig. 5(b) shows no observable orbital polarization. The absence of linear dichroism indicates no splitting of e_g orbitals as expected for undistorted octahedra in bulk crystal. The observed electronic structure suggests the presence of *uniform* Ni-O bond lengths despite the 1.8% tensile strain,[7,30] and a c-axis lattice parameter with a small contraction in the out-of-plane direction. The data shown here is for bulk sensitive FY, but the surface sensitive total electron yield (TEY) displays the same response. This indicates that the bulk of the film and the surface have a similar orbital configuration. This is consistent with the fact that the tilts should be representative of the entire film. While the tilt pattern might be modified within ~2–3 uc of the STO interface,[11] the average of the entire film is the dominant signal.

C. Atomic structure–electronic function analysis

To reconcile this discrepancy, we emphasize that the presence or absence of linear dichroism should be directly attributed to the flavor of structural distortions in NNO and LNO films, which originate from intrinsic ferroelastic tendencies of the bulk phases. To establish this relationship, we adapt an approach based on distortion modes[36,37] which provides a description of the distorted strained structures in terms of irreducible representations (irreps), i.e., static structural displacements, of the ideal cubic perovskite phase. For an ideal cubic structure, each irrep within this basis has zero amplitude. However, the irreps compatible with the symmetry breaking from cubic ($Pm\bar{3}m$) to $C2/c$ and $Pbnm$ acquire finite amplitudes.

In the RNiO$_3$ perovskites, three symmetry-unique irreps describe the common octahedral distortions: (i) NiO$_6$ octahedral rotations (R_4^+ and M_3^+), (ii) Jahn-Teller distortions (R_3^+ and M_2^+), which lift the e_g degeneracy leading to orbital polarization, and (iii) NiO$_6$ breathing distortions (R_1^+), which causes the octahedra to dilate or contract according to the magnitude of charge δ transferred between Ni sites.[38] We hypothesize that the XLD seen in NNO films [Fig. 5(a)] requires the presence of local Jahn-Teller distortions to the NiO$_6$ octahedra. To confirm this relationship between crystal symmetry and orbital polarization, we use the ISODISTORT package[36] to decompose the LNO and NNO films' crystal structure obtained from density functional calculations and make a comparison to their bulk equilibrium phases in terms of these irreps.

1. *Groundstate NdNiO$_3$ structures*

The ground state structure for NNO on STO substrates was determined from density functional calculations within the spin-polarized generalized gradient approximation (GGA) PBEsol exchange-correlation functional[39] plus Hubbard-U method as implemented in the Vienna ab initio simulation package (VASP).[40–43] In our simulations, we do not explicitly include the substrate but rather impose the mechanical constraint that the in-plane lattice parameters are fixed to those of the experimental lattice constant of STO and the out-of-plane lattice constant is given by our experimental measurements. We then optimize the internal degrees of freedom. The Dudarev approach[41] was followed to include an effective Hubbard term $U_{\text{eff}} = U\text{-}J$ of 4 eV and accurately treat the correlated Ni $3d$ orbitals. The core and valence electrons were treated with the projector-augmented wave method,[44] and the Brillouin-zone integrations were performed with a Gaussian smearing of 0.05 eV over a 7 × 7 × 7 Monkhorst-Pack k-point mesh[45] centered at Γ, and a 500 eV plane-wave cutoff. In all calculations, ferromagnetic spin order was imposed.

We surveyed four NNO crystal structures belonging to space groups $P\bar{1}$, $P2_1/m$, $P2_1/c$, and $Pnma$ informed by symmetry-breaking selection rules and calculated the equilibrium geometry to determine the ground state structure

TABLE I. Energy difference (ΔE) obtained from DFT calculations of NNO on STO substrates for in-phase octahedral rotations either parallel (‖) or perpendicular (⊥) to the plane of epitaxial strain. ΔE is given in meV/f.u.

Space group	Orientation	ΔE (meV/f.u.)
$P\bar{1}$	‖	11.315
$P2_1/m$	‖	17.55
$P2_1/c$	⊥	**0**
$Pnma$	⊥	7.86

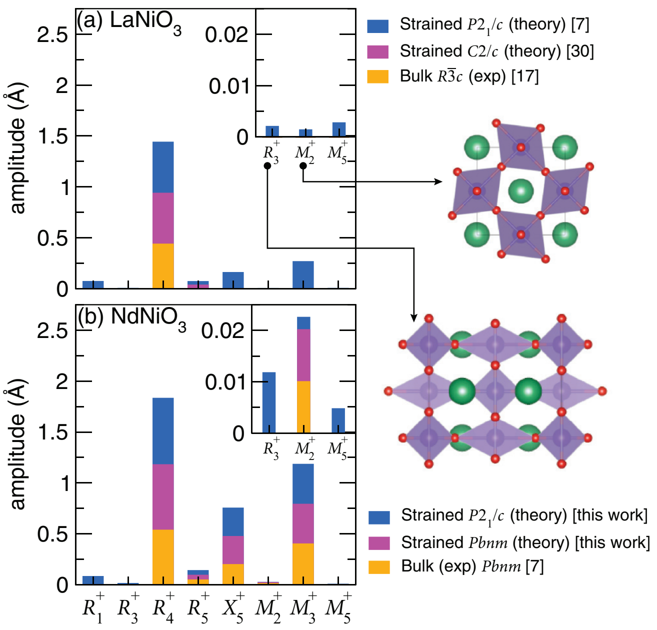

FIG. 6. (Color online) Distortion-mode analysis of (a) LNO and (b) NNO structures in both thin film and bulk phases with bond elongation modes producing orbital polarizations shown schematically to the right.

for NNO on STO substrate. In symmetries $P\bar{1}$ and $P2_1/m$ the long axis about which the in-phase rotations of octahedra occur is oriented parallel (‖) to the epitaxial plane, whereas in $P2_1/c$ and $Pnma$ the long axis is perpendicular (⊥) to the epitaxial plane. The crystal structure data for all relaxed configurations can be found in Ref. 38 and Supplemental Material[46]. For NNO we find that the lowest energy structure belongs to monoclinic $P2_1/c$ symmetry (Table I), thereby favoring in-phase octahedral rotations that occur about an axis perpendicular to the epitaxial plane concommitant with breathing distortions of the NiO$_6$ units. The next lowest energy structure exhibits essentially the same octahedral tilt pattern, but lacks the later breathing distortion.

2. Symmetry-adapted mode decompositions

The LNO films on STO with $C2/c$ monoclinic structure are decomposed into R_4^+ and R_5^+ [Fig. 6(a)] irreps associated with the out-of-phase octahedral rotations and out-of-phase bending mode, respectively (a schematic representation of symmetry-adapted distortion modes can be found in Supplemental Material[46]). In bulk LNO, however, the rhombohedral $R\bar{3}c$ symmetry[17] prohibits the R_5^+ and consists of only the R_4^+ mode. This analysis also finds a key structural feature missing: Despite the tetragonal strain on the crystal lattice, we do not find any NiO$_6$ Jahn-Teller mode in the LNO films, which supports the observed absence of dichroism in our polarized XAS measurements [Fig. 5(c)]. Note that although earlier work[7] showed that LNO films under tensile strain on STO at low temperature show a semiconducting gap of 0.10 eV (space group $P2_1/c$), stabilized by an emergent strain-induced octahedral breathing distortion not found in the bulk, the relatively small amplitudes of the Jahn-Teller irreps M_2^+ and R_3^+ [Fig. 6 (inset)] should also lead to no appreciable dichroism.

In the case of NNO on STO thin films, our experimental results suggest the same orthorhombic $Pbnm$ symmetry as in the bulk, albeit with modified internal coordinates. These NNO phases are decomposed into five irreps [Fig. 6(b)] with the only difference between bulk NNO and thin film NNO being that the thin film NNO is relatively more distorted than the bulk phase. Note that our zero-kelvin DFT calculations identified $P2_1/c$ as the ground-state crystal structure for homoepitaxially strained NNO under experimentally determined lattice parameters, consistent with the experimental structure at low temperature.[38] In Fig. 6(b), we compare the relative distortion-mode amplitudes of NNO on STO thin films and bulk NNO (RT phase). In all cases, we find large and finite amplitudes for the M_2^+ Jahn-Teller mode in NNO on STO film with $P2_1/c$ symmetry; we also detect a relatively large amplitude for R_3^+ Jahn-Teller mode. It is the presence of these dominant Jahn-Teller distortions in the NNO thin films that produce the large dichroism and orbital polarization [Fig. 5(a)].

Therefore, our distortion-mode analysis clearly discerns the difference in the lattice response of LNO and NNO thin films subjected to large epitaxial tensile strain. The propensity for orbital polarization in RNiO$_3$ thin films is strongly influenced by the crystal symmetry of bulk materials. In NNO thin films and bulk, we find clear evidence of Jahn-Teller distortions present, suggesting that further distortions of this type due to epitaxial constraints would cost small (if any) energy. It appears rather that bulk orthorhombic nickelates without regular NiO$_6$ octahedra and bond distortions prefer to accommodate epitaxial strain through additional bond elongations and contractions. In sharp contrast, the absence of orbital polarization in LNO films with regular NiO$_6$ octahedra is directly attributed to its bulk ground-state structure (space group $R\bar{3}c$), where the Jahn-Teller modes are *prohibited by symmetry*. In this case, strain-induced Jahn-Teller distortions would likely result in large energetic penalties.

IV. SUMMARY

In summary, using a combination of high-resolution x-ray diffraction, polarization-dependent soft x-ray absorption spectroscopy, and a quantitative group theoretical analysis computed from DFT, we report that the preferred orbital configurations adopted by the thin films is the one that stays closest to the bulk, suggesting the strain-stabilized phases retain a "memory" of their bulk state. We suggest that knowledge of the structural distortions present in the bulk thermodynamic phases emerges as an essential and critical descriptor to guide materials selection for epitaxial thin films with desired orbital polarizations. Additional studies of different symmetry mismatch under different strain of perovskites should be done to advance our understanding for the rational design of heterostructure materials with orbital-lattice interaction.

ACKNOWLEDGMENTS

Portions of this work were performed at the DuPont-Northwestern-Dow Collaborative Access Team (DND-CAT), which is supported by E.I. DuPont de Nemours & Co., The Dow Chemical Company, and Northwestern University. Work at the Advanced Photon Source is supported by the

US Department of Energy, Office of Science under Grant No. DEAC02-06CH11357. J. Chakhalian was supported by DOD-ARO under the Grant No. 0402-17291 and NSF Grant No. DMR-0747808. P.V.B. and J.M.R. were supported by DARPA under the Grant No. N66001-12-4224. DFT calculations were carried out at the high-performance computing cluster (CARBON) of the Center for Nanoscale Materials (Argonne National Laboratory) supported by the US DOE, Office of Science, Office of Basic Energy Sciences, under Contract No. DE-AC02-06CH11357.

---

[*] ichengtung@u.northwestern.edu

[†] Present address: Department of Physics, University of California, Berkeley, California 94720, USA.

[‡] freeland@anl.gov

[1] J. Chakhalian, A. J. Millis, and J. M. Rondinelli, Nat. Mater. **12**, 92 (2012).

[2] J. M. Rondinelli and N. A. Spaldin, Adv. Mater. **23**, 3363 (2011).

[3] J. Chaloupka and G. Khaliullin, Phys. Rev. Lett. **100**, 016404 (2008).

[4] P. Hansmann, X. Yang, A. Toschi, G. Khaliullin, O. K. Andersen, and K. Held, Phys. Rev. Lett. **103**, 016401 (2009).

[5] P. Hansmann, A. Toschi, X. Yang, O. K. Andersen, and K. Held, Phys. Rev. B **82**, 235123 (2010).

[6] Y. Tokura and N. Nagaosa, Science **288**, 462 (2000).

[7] J. Chakhalian, J. M. Rondinelli, Jian Liu, B. A. Gray, M. Kareev, E. J. Moon, N. Prasai, J. L. Cohn, M. Varela, I. C. Tung, M. J. Bedzyk, S. G. Altendorf, F. Strigari, B. Dabrowski, L. H. Tjeng, P. J. Ryan, and J. W. Freeland, Phys. Rev. Lett. **107**, 116805 (2011).

[8] J. W. Freeland, J. Liu, M. Kareev, B. Gray, J. W. Kim, P. J. Ryan, R. Pentcheva, and J. Chakhalian, Europhys. Lett. **96**, 57004 (2011).

[9] A. V. Boris, Y. Matiks, E. Benckiser, A. Frañó, P. Popovich, V. Hinkov, P. Wochner, M. Castro-Colin, E. Detemple, V. K. Malik, C. Bernhard, T. Prokscha, A. Suter, Z. Salman, E. Morenzoni, G. Cristiani, H.-U. Habermeier, and B. Keimer, Science **332**, 937 (2011).

[10] E. Benckiser, M. W. Haverkort, S. Brück, E. Goering, S. Macke, A. Frañó, X. Yang, O. K. Andersen, G. Cristiani, H.-U. Habermeier, A. V. Boris, I. Zegkinoglou, P. Wochner, H.-J. Kim, V. Hinkov, and B. Keimer, Nat. Mater. **10**, 189 (2011).

[11] J. M. Rondinelli, S. J. May, and J. W. Freeland, MRS Bull. **37**, 261 (2012).

[12] M. L. Medarde, J. Phys.: Condens. Matter **9**, 1679 (1997).

[13] M. Medarde, J. Mesot, S. Rosenkranz, P. Lacorre, W. Marshall, S. Klotz, J. S. Loveday, G. Hamel, S. Hull, and P. Radaelli, Physica B **234–236**, 15 (1997).

[14] J. B. Torrance, P. Lacorre, A. I. Nazzal, E. J. Ansaldo, and C. Niedermayer, Phys. Rev. B **45**, 8209 (1992).

[15] J. Liu, M. Kareev, B. Gray, J. W. Kim, P. J. Ryan, B. Dabrowski, J. W. Freeland, and J. Chakhalian, Appl. Phys. Lett. **96**, 233110 (2010).

[16] R. Scherwitzl, P. Zubko, I. G. Lezama, S. Ono, A. F. Morpurgo, G. Catalan, and J.-M. Triscone, Adv. Mater. **22**, 5517 (2010).

[17] J. L. García-Muñoz, J. Rodríguez-Carvajal, P. Lacorre, and J. B. Torrance, Phys. Rev. B **46**, 4414 (1992).

[18] J. Liu, M. Kareev, S. Prosandeev, B. Gray, P. J. Ryan, J. W. Freeland, and J. Chakhalian, Appl. Phys. Lett. **96**, 133111 (2010).

[19] D. H. A. Blank, G. Koster, G. A. J. H. M. Rijnders, E. van Setten, P. Slycke, and H. Rogalla, J. Cryst. Growth **211**, 98 (2000).

[20] M. Kareev, S. Prosandeev, J. Liu, C. Gan, A. Kareev, J. W. Freeland, M. Xiao, and J. Chakhalian, Appl. Phys. Lett. **93**, 061909 (2008).

[21] J. W. Freeland, J. C. Lang, G. Srajer, R. Winarski, D. Shu, and D. M. Mills, Rev. Sci. Instrum. **73**, 1408 (2002).

[22] P. A. Fenter, Rev. Mineral. Geochem. **49**, 149 (2002).

[23] U. Gebhardt, N. V. Kasper, A. Vigliante, P. Wochner, H. Dosch, F. S. Razavi, and H.-U. Habermeier, Phys. Rev. Lett. **98**, 096101 (2007).

[24] A. Vailionis, H. Boschker, W. Siemons, E. P. Houwman, D. H. A. Blank, G. Rijnders, and G. Koster, Phys. Rev. B **83**, 064101 (2011).

[25] R. Scherwitzl, P. Zubko, C. Lichtensteiger, and J.-M. Triscone, Appl. Phys. Lett. **95**, 222114 (2009).

[26] S. S. Lee, C. Park, P. Fenter, N. C. Sturchio, and K. L. Nagy, Geochim. Cosmochim. Acta. **74**, 1762 (2010).

[27] W. H. Press, *Numerical Recipes: The Art of Scientific Computing*, 3rd ed. (Cambridge University Press, Cambridge, 2007).

[28] S. J. May, C. R. Smith, J. W. Kim, E. Karapetrova, A. Bhattacharya, and P. J. Ryan, Phys. Rev. B **83**, 153411 (2011).

[29] A. M. Glazer, Acta. Cryst. A **31**, 756 (1975).

[30] S. J. May, J. W. Kim, J. M. Rondinelli, E. Karapetrova, N. A. Spaldin, A. Bhattacharya, and P. J. Ryan, Phys. Rev. B **82**, 014110 (2010).

[31] C. L. Jia, S. B. Mi, M. Faley, U. Poppe, J. Schubert, and K. Urban, Phys. Rev. B **79**, 081405(R) (2009).

[32] A. Y. Borisevich, H. J. Chang, M. Huijben, M. P. Oxley, S. Okamoto, M. K. Niranjan, J. D. Burton, E. Y. Tsymbal, Y. H. Chu, P. Yu, R. Ramesh, S. V. Kalinin, and S. J. Pennycook, Phys. Rev. Lett. **105**, 087204 (2010).

[33] J. Hwang, J. Y. Zhang, J. Son, and S. Stemmer, Appl. Phys. Lett. **100**, 191909 (2012).

[34] J.-S. Zhou and J. B. Goodenough, Phys. Rev. B **69**, 153105 (2004).

[35] K. H. Ahn, T. Lookman, and A. R. Bishop, Nature (London) **428**, 401 (2004).

[36] B. J. Campbell, H. T. Stokes, D. E. Tanner, and D. M. Hatch, J. Appl. Cryst. **39**, 607 (2006).

[37] J. M. Perez-Mato, D. Orobengoa, and M. I. Aroyo, Acta Cryst. A **66**, 558 (2010).

[38] P. V. Balachandran and J. M. Rondinelli, Phys. Rev. B **88**, 054101 (2013).

[39] J. P. Perdew, A. Ruzsinszky, G. I. Csonka, O. A. Vydrov, G. E. Scuseria, L. A. Constantin, X. Zhou, and K. Burke, Phys. Rev. Lett. **100**, 136406 (2008).

[40] V. I. Anisimov, F. Aryasetiawan, and A. I. Liechtenstein, J. Phys.: Condens. Matter **9**, 767 (1997).

[41] S. L. Dudarev, G. A. Botton, S. Y. Savrasov, C. J. Humphreys, and A. P. Sutton, Phys. Rev. B **57**, 1505 (1998).

[42] G. Kresse and J. Furthmüller, Phys. Rev. B **54**, 11169 (1996).

[43] G. Kresse and D. Joubert, Phys. Rev. B **59**, 1758 (1999).

[44] P. E. Blochl, Phys. Rev. B **50**, 17953 (1994).

[45] H. J. Monkhorst and J. D. Pack, Phys. Rev. B **13**, 5188 (1976).

[46] See Supplemental Material at http://link.aps.org/supplemental/10.1103/PhysRevB.88.205112 for additional details of structural data and irreducible representations.